

RADAR STUDIES OF AVIATION HAZARDS: Part 2 Lightning Precursors

**F. Ian Harris
David J. Smalley
Shu-Lin Tung
Alan R. Bohne**

**Hughes STX Corporation
c/o OL-AA PL/GPAB
29 Randolph Rd.
Hanscom AFB, MA 01731-3010**

15 July 1996

19970206 117

Scientific Report No. 3

DTIC QUALITY INSPECTED 3/

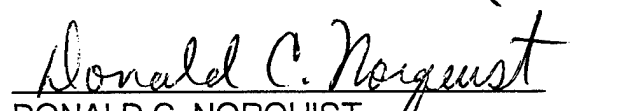
APPROVED FOR PUBLIC RELEASE; DISTRIBUTION UNLIMITED.

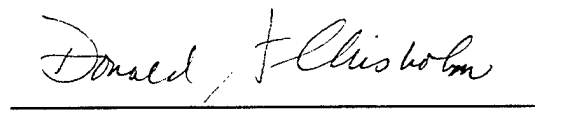


**PHILLIPS LABORATORY
Directorate of Geophysics
AIR FORCE MATERIEL COMMAND
HANSCOM AIR FORCE BASE, MA 01731-3010**

"This technical report has been reviewed and is approved for publication."


PAUL R. DESROCHERS
Contract Manager


DONALD C. NORQUIST
Acting Chief, Satellite Analysis and Weather
Prediction Branch
Atmospheric Sciences Division


DONALD A. CHISHOLM, Acting Director
Atmospheric Sciences Division

This report has been reviewed by the ESC Public Affairs Office (PA) and is releasable to the National Technical Information Service (NTIS).

Qualified requestors may obtain additional copies from the Defense Technical Information Center (DTIC). All others should apply to the National Technical Information Service (NTIS).

If your address has changed, or if you wish to be removed from the mailing list, or if the addressee is no longer employed by your organization, please notify PL/IM, 29 Randolph Road, Hanscom AFB, MA 01731-3010. This will assist us in maintaining a current mailing list.

Do not return copies of this report unless contractual obligations or notices on a specific document requires that it be returned.

REPORT DOCUMENTATION PAGE			Form Approved OMB No. 0704-0188	
Public reporting burden for this collection of information is estimated to average 1 hour per response, including the time for reviewing instructions, searching existing data sources, gathering and maintaining the data needed, and completing and reviewing the collection of information. Send comments regarding this burden estimate or any other aspect of this collection of information, including suggestions for reducing this burden, to Washington Headquarters Services, Directorate for Information Operations and Reports, 1215 Jefferson Davis Highway, Suite 1204, Arlington, VA 22202-4302, and to the Office of Management and Budget, Paperwork Reduction Project (0704-0188), Washington, DC 20503.				
1. AGENCY USE ONLY (Leave blank)		2. REPORT DATE 15 July 1996		3. REPORT TYPE AND DATES COVERED Scientific No. 3
4. TITLE AND SUBTITLE RADAR STUDIES OF AVIATION HAZARDS: Part 2. Lightning Precursors			5. FUNDING NUMBERS F19628-93-C-0054 PE63707F PR 2781 TA GT WU MA	
6. AUTHOR(S) F. Ian Harris, David J. Smalley, Shu-Lin Tung, and Alan R. Bohne				
7. PERFORMING ORGANIZATION NAME(S) AND ADDRESS(ES) Hughes STX Corporation c/o OL-AA PL/GPAB 29 Randolph Road Hanscom AFB, MA 01731-3010			8. PERFORMING ORGANIZATION REPORT NUMBER Hughes STX Scientific Report #9	
9. SPONSORING/MONITORING AGENCY NAME(S) AND ADDRESS(ES) Phillips Laboratory 29 Randolph Road Hanscom AFB, MA 01731-3010 Contract Manager: Paul R. Desrochers/GPAB			10. PERFORMING ORGANIZATION REPORT NUMBER PL-TR-96-2178(II)	
11. SUPPLEMENTARY NOTES				
12a. DISTRIBUTION/AVAILABILITY STATEMENT Approved for public release; distribution unlimited			12b. DISTRIBUTION CODE	
13. ABSTRACT (Maximum 200 words) Automated techniques have been developed to detect the three-dimensional structure of convective storms as a tool for the prediction of the onset of lightning.				
14. SUBJECT TERMS Doppler weather radar, automated techniques, lightning precursors, storm structure, storm mass, storm volume			15. NUMBER OF PAGES 32	
			16. PRICE CODE	
17. SECURITY CLASSIFICATION Unclassified	18. SECURITY CLASSIFICATION OF THIS PAGE Unclassified	19. SECURITY CLASSIFICATION OF ABSTRACT Unclassified	20. LIMITATION OF ABSTRACT Unclassified	

Table of Contents

1	INTRODUCTION	1
2	EXTRACTABLE STORM STRUCTURES	2
3	ALGORITHM	3
3.1	Methodology	3
3.2	Preprocessing	4
3.3	Structure Computations	5
4	ANALYSIS	6
4.1	May 16, 1995 Dodge City, KS	7
4.2	May 12, 1995 Goodland, KS	18
5	SUMMARY	27
6	REFERENCES	28

1 INTRODUCTION

For convective storms developing in a weakly sheared environment, considerable evidence has been amassed that relates radar reflectivity structure and lightning activity. Marshall and Radhakant (1978) suggest that the electrical activity of thunderstorms is related to radar reflectivity observed at the 6-7 km level. This idea was further tested by Lhermitte and Krehbiel (1979). They horizontally integrated the radar reflectivity of a storm at several heights and found that lightning began when the storm top reached 8 km (-20°C). Also, they found that the peak flash rate (about 1 flash/s) occurred when the reflectivity exceeded 50 dBZ at the -10°C level. Buechler and Goodman (1991) observed that cloud-to-ground strikes began when the reflectivity values of 30-40 dBZ extended above 7 km. While all the above observations were made in Florida, similar altitude or temperature thresholds were found in New Mexico (Krehbiel, 1986) and the tropics (Williams, 1991). Other studies have looked at various methods of comparing reflectivity data and lightning activity. A recent study by Harris-Hobbs *et al* (1992) attempted to correlate lightning activity with storm volumes exceeding various thresholds. They found good correlations between the magnitudes of the volumes exceeding 20 dBZ and flash activity. However, for some of their data, regions with higher reflectivity thresholds attain peak volumes before that for the 20 dBZ threshold and before the time of maximum lightning activity. This suggests another prediction tool, but it should be noted that most other observations indicate that lightning activity is directly proportional to the storm mass. It should be apparent that many workers have found relationships between the structure of reflectivity factors and the onset of lightning activity. However, no clear criteria have been established because most of the conclusions have been based on limited case studies. With routine data collections from WSR-88D systems, more definitive criteria should now be possible.

The overall goal of this effort is to develop a technique that will yield predictions of lightning initiation for air mass thunderstorms. An algorithm has been developed that evaluates the reflectivity factor structure of storms and provides automated statistics for subsequent analysis. While the algorithm has been established there have been difficulties in securing lightning data. As a consequence, the algorithm has been applied to two convective storm complexes with results compared with the occurrence of hail and tornadoes.

Assessment of the potential for lightning prediction will proceed after receipt of lightning data from the National Lightning Detection Network (NLDN).

2 EXTRACTABLE STORM STRUCTURES

With Doppler radar, the three dimensional structure of storms can be observed as a function of time. To get the most information from these data, it would seem reasonable to treat them from a four-dimensional perspective. One approach, the one adopted for this development, is to extract three-dimensional characteristics of the precipitation structures of storms and to depict and analyze these as a function of time. The focus should be on those features most associated with lightning initiation as outlined in the previous section. However, as will become apparent, these extracted features may also be useful in the evaluation of the potential for other severe weather events. Examples of structures that can be extracted from each volume are:

- Overall storm parameters
 - Storm mass above specified thresholds using an assumed reflectivity factor - liquid water content relationship.
 - Storm volume above specified thresholds
 - Storm centroids
 - Storm (echo) top
 - Maximum reflectivity location and magnitude
- Vertical profiles within storms:
 - Precipitation mass per unit depth within layers at specified heights and/or thicknesses.
 - Area within a specified reflectivity threshold within layers at specified heights and/or thicknesses.
 - Centroids of layers

Collectively, when viewed in time, these parameters will give a reasonably comprehensive four-dimensional perspective of convective storms. From the vertical profiles, an evaluation of the amount of precipitation that there is in the storm above a specific temperature level is readily derived. Also, it is perceived that the volumetric and areal relationships are likely to be more reliable predictors than individual estimates of parameters such as reflectivity factor as suggested by other workers cited earlier.

3 ALGORITHM

3.1 Methodology

Radar data are collected in spherical coordinates, an unnatural framework for the analysis of meteorological phenomena. As a result, a remapping of data or results is required for interpretation purposes. This remapping can be performed on the original raw data or at some point further into the processing. The procedure adopted here is to retain the data in their original framework and to compile analyses in the form of volumetric and layer statistics organized in a more logical storm reference system. In this case, a rectangular Cartesian coordinate system has been adopted for the storm reference system. The layer statistics are computed for horizontal slabs with bases at height h_b above the curved surface of the earth and of constant but specifiable depth d . These depths are either optimized for each volume scan or are selected by the analyst. Statistics are then produced for assessment for temporal evolution on a layer or storm basis.

Typically, data are collected at 1 km intervals in range and 1° in azimuth on planes of constant elevation angle. The elevation angles are increased from about 0.5° to an upper limit at intervals that are specified according to the phenomena being observed. The elevation angle intervals are usually irregular and provide the "best" compromise between spatial and temporal resolution. Because the data are collected in spherical space, the resolvable scales in rectangular Cartesian space increase with increasing range. In addition, the radar sampling volume (the convolution of the radar pulse volume with the sampling function) also increases with range. As will be seen, these factors are considered in the design and implementation of the layer and volume analysis procedures.

The analysis consists of the following procedures:

- Preprocessing
 - Crop data to vicinity of storm
 - Threshold data
 - Compute derived field
 - Compute pulse volume
- Storm structure computations
 - Placement of data into layers
 - Computation of layer and volume statistics

Each of these processing steps will now be described.

3.2 Preprocessing

As noted above, there are several steps involved in this stage of processing. The first step involves the focusing of the analysis upon the storm of interest. Currently, this is done manually but will be automated in the future. This process is required to reduce the data volume to be processed and to allow the assessment on a storm-by-storm basis.

Once the data are focused, a threshold is applied to the reflectivity factor data to further remove extraneous echoes. Typically, a value of 15 dBZ is used, but this value is easily changed to accommodate a particular data set or analyst. Once data below this threshold are removed, all subsequent computations are confined to the remaining data values.

In order to estimate precipitation mass, a method of converting reflectivity factor to liquid water content is required. Mass is computed with an assumed relationship ($Z_e = aM^b$) where Z_e and M are the radar measured reflectivity factor (in mm^6m^{-3}) and liquid water content (in g m^{-3}) respectively. The values of a and b are specifiable by the analyst. Typical values are $a = 31500$ and $b = 1.41$, reasonable values for thunderstorms. While the numerical values of the resultant masses are very dependent upon the values of a and b that are adopted, the impact on the assessment of the temporal variability is relatively inconsequential. It

should be noted that there is substantial variability to a and b on all scales. They vary amongst geographic regions, amongst seasons, amongst storms, amongst stages of storm development, and even within a single storm at a given time. It would therefore appear to be relatively futile to adopt a more sophisticated assessment of a and b values to account for this variability. Besides, this technique does not focus on the actual values of the liquid water estimates but is more concerned with the trends. As a result, it is intended to select one set of values (a=31500, b = 1.41) for all processing.

Computation of pulse volume parameters such as volume, mass, location, horizontal area, and vertical thickness are central to the subsequent analyses. The pulse volume is assumed to be a subsection of a cone centered at the radar and its volume (V_p) is defined by the formula:

$$V_p \approx \pi \theta_0^2 \phi_0^2 R^2 \Delta h$$

where R is range from the radar to the center of the pulse volume, Δh is the volume depth in meters, θ_0 and ϕ_0 are the halfpower horizontal and vertical beamwidths, respectively. Beam positions are determined from the spherical coordinates of the beam where the height is corrected for earth's curvature with the standard 4/3 earth radius approximation .

3.3 Structure Computations

The analysis domain is specified by the analyst in terms of minimum and maximum heights. This allows the analyst to examine the storm within certain height constraints that conform to specific temperature regimes that are perceived to be important for the assessment of lightning initiation. The domain is then divided into layers where layer thickness may be user specified or determined from an "optimum thickness" calculation for each radar volume based on range and data resolution. When optimization is performed for each volume scan, there can be considerable variations in layer thickness as the storm progresses across the radar scanning domain. Therefore, as will be seen shortly, normalization of layer data to unit (1 km) thicknesses is required for meaningful intra-volume comparisons.

Data are placed within a layer based on the location of the center of the pulse volume. That is, if the volume center is within the layer, the entire volume is considered to also be

within the slab. The volumes are then accumulated within each slab and the subsequent volume is normalized by the thickness of the slab to yield a layer area.

For mass computations, the liquid water content (g m^{-3}) values derived from an assumed Z - M relationship that has been applied to the reflectivity data are then multiplied by the data volume, assigned to a layer, and accumulated within that assigned slab. Once accumulation is complete for all layers, masses are further accumulated to produce a storm water mass estimate. The layer masses are then normalized by the thickness of the layer.

Mass-weighted and volume-weighted centroids are computed for each slab with the function

$$\bar{x}_i = \frac{\sum_{slab} x_{i,j} F_j}{\sum_{slab} F_j}$$

where x_i is one of the three rectangular Cartesian coordinates (x,y,z) and F_j is the volume or mass within the sampling volume. Summations are performed for all sampling volumes centered within the layer for layer centroids and within the volume for volume thresholds.

4 ANALYSIS

As a test of the analysis techniques, data from two storms were processed for periods of more than 5 hours each. While no lightning data is yet available for these storms, the evolution of the storms will be demonstrated and related to severe weather. During the next year, once lightning data have been obtained, analyses of the radar and lightning data will be compared to assess the appropriateness for lightning prediction.

4.1 *May 16, 1995 Dodge City, KS*

This storm developed to the West of the Dodge City, KS, WSR-88D radar and subsequently moved toward the east-northeast, producing several tornadoes and significant hail. Radar data were processed from very early in the life of this storm until the storm was approaching the edge of the practicable working area, a period of about 325 minutes. The

various statistics discussed earlier were computed and the results assessed.

Figures 1 and 2 are bubble plots indicating the growth and motion of the storm with time, where the storm is moving from left to right. Each bubble represents the volume (Figure 1) or mass (Figure 2) of the storm contained within the 15 dBZ isosurface for one volume scan. The bubble volume is directly proportional to the volume or mass of the storm. The center of the bubble is located at the three-dimensional storm centroid. Note how the storm undergoes rapid growth in volume (Figure 1) during its early life (on the lower left of this figure) and again towards the end (on the upper right). The mass (Figure 2) also has two distinct maxima, coinciding with those of the volume data. There are two other growth periods for the mass between those two that are not as distinguishable in the volume plot. Note that storm mass is maximized much earlier than the volume.

One of the features of the structure assessment module is that the storm can be divided into layers for vertical structure assessment. Figure 3 presents plots of the area and mass within layers of the storm as a function of time and height. In this figure the largest areas or mass are the lightest in shading. Time progresses to the right and encompasses 325 minutes. In the area profile, we see that the area maxima tend to occur at mid-levels. However, we see regions of maxima that extend from upper left toward the lower right (e.g., between 60 and 90 minutes and between 120 and 150 minutes). These are indicative of bursts of precipitation generated aloft that subsequently descend and continue to grow. There is a periodicity to these bursts of the order of 15 to 30 minutes, typical time scales for convection. The mass portion of this figure suggests that the main maxima are in the lower levels of the storm, with secondary maxima at mid- to high-levels. There is a tendency for the maxima in mass and area to be somewhat correlated in time but not necessarily with height. These configurations for the volume and mass are typical of convective storms.

Volume

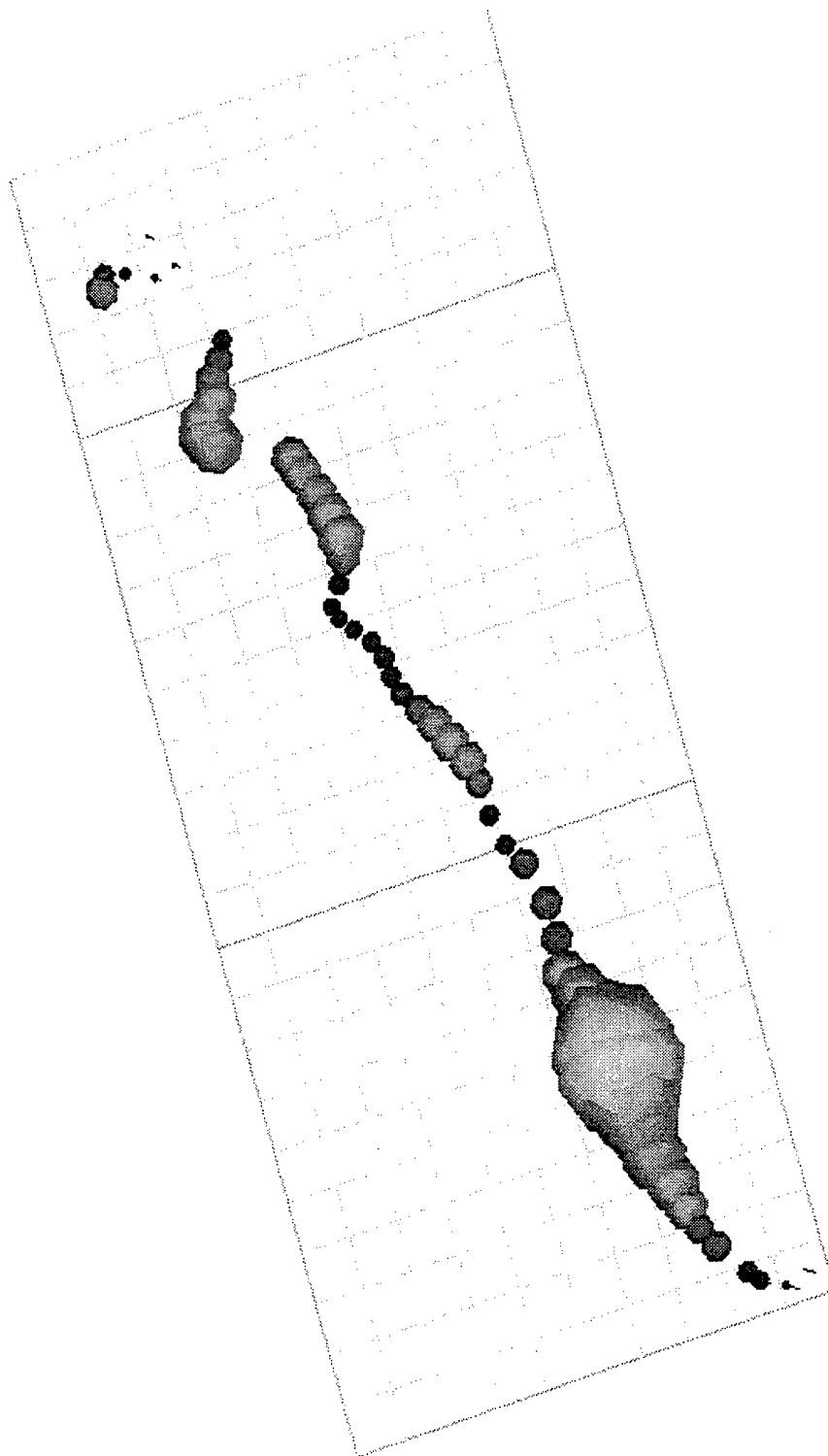


Figure 1. Plot of mass-weighted centroid locations. Each grid box (small) is 10 km by 10 km. Bubble radius is proportional to storm volume. Data are for Dodge City data for May 16-17, 1995.

Mass

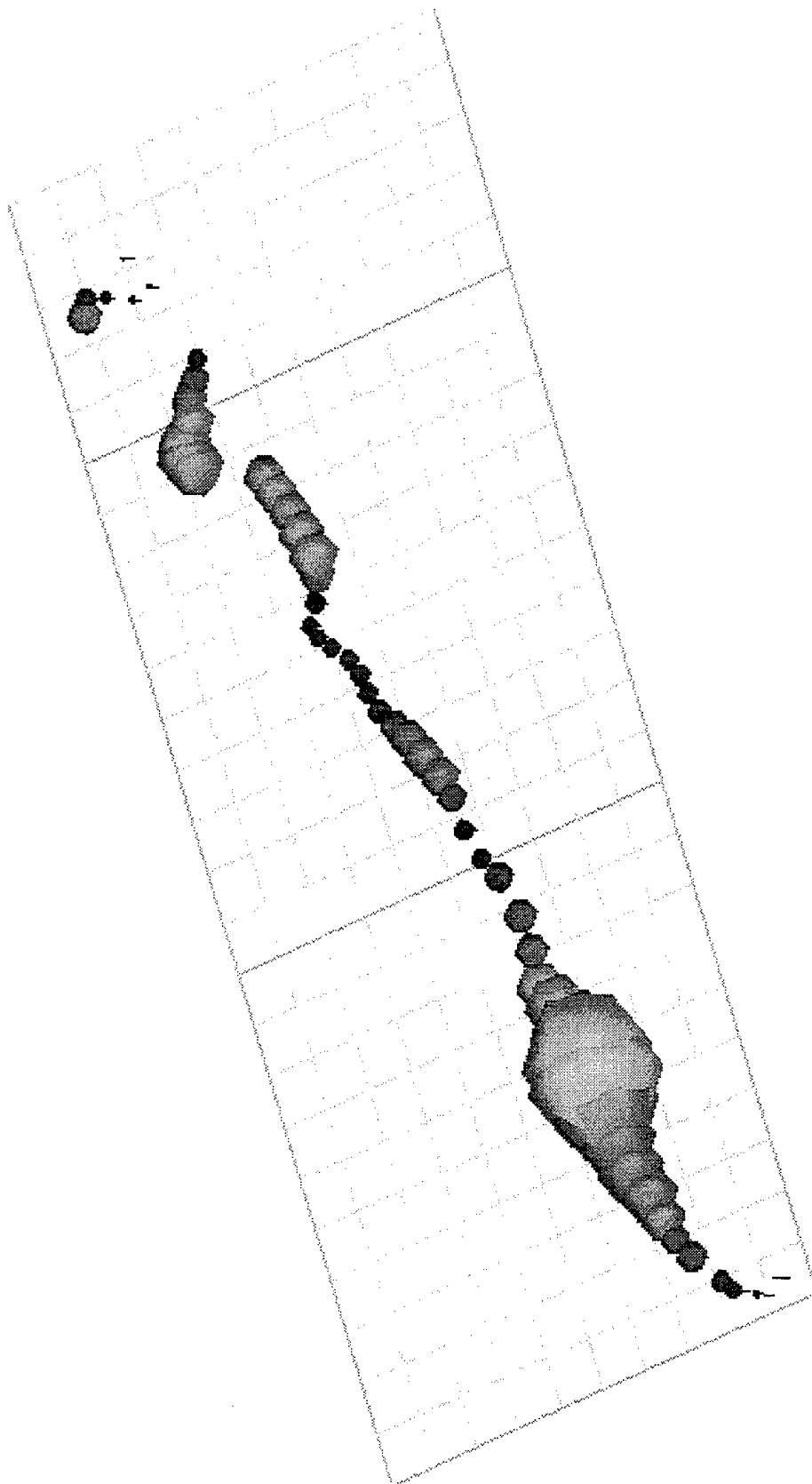


Figure 2. As in Figure 1 but where bubble radius is proportional to precipitation mass within storm.

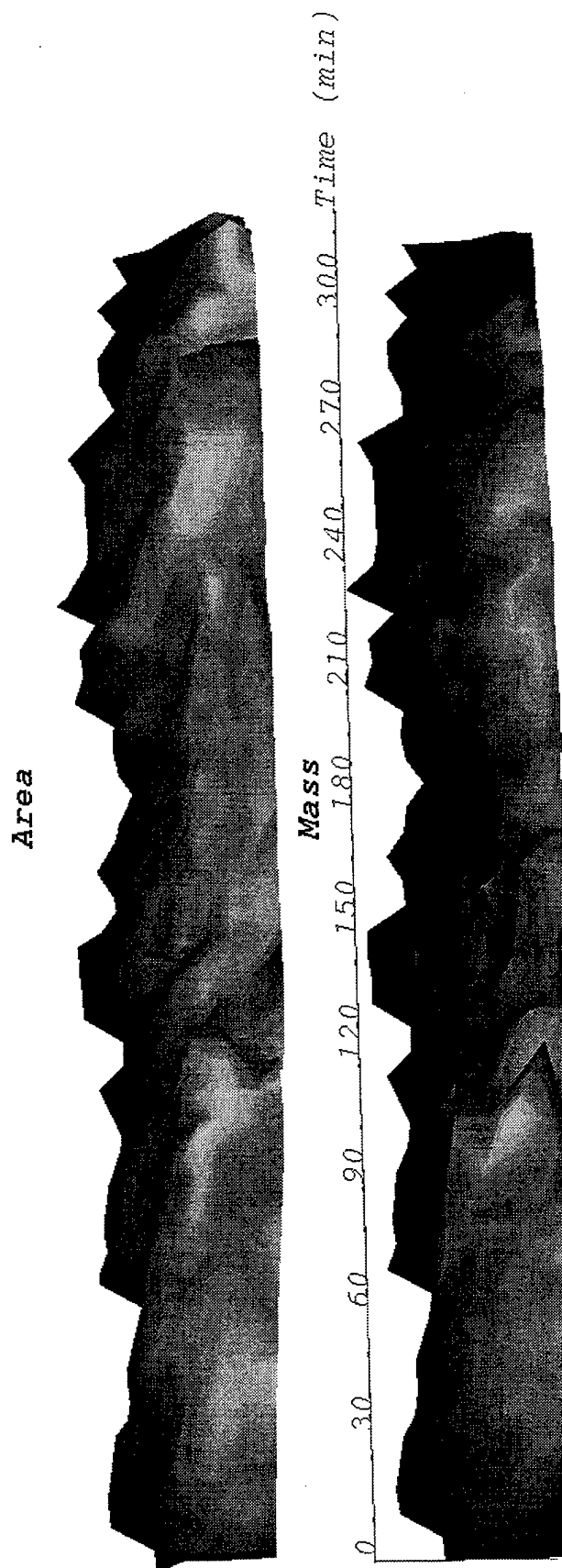


Figure3 Plot of area and mass of layers within storm as a function of height and time. Time scale is in minutes. Shading of each profile is such that light indicates high values and dark indicates low. Time is relative to that of the first radar volume processed. Data are for Dodge City data for May 16-17.

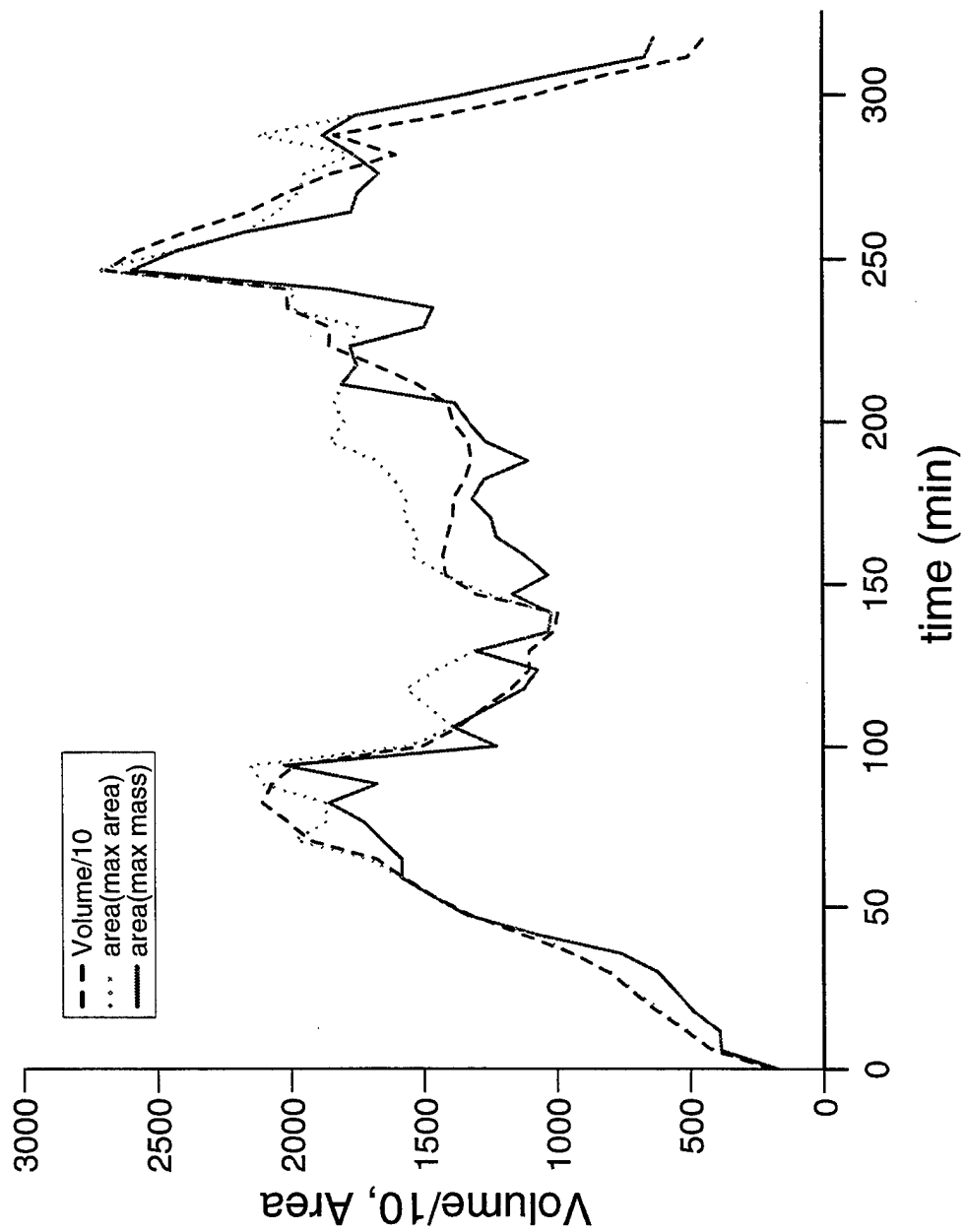


Figure 4. Plot of storm volume divided by 10 and areas of the layers where the areas and mass are maxima as a function of time. Data are for Dodge city on May 16-17. Time is as in Figure 3.

Figure 4 presents the variations of the storm volume and of the areas at the levels where the area (max area) and mass (max mass) are the greatest. As would be expected, these three parameters track well with each other, particularly with regard to the larger scales. There is a sharp increase in all three curves for the first approximately 75 minutes, followed by a general decline for the next 75 minutes. Subsequent to the decline there is another increase to a pronounced maximum about 260 minutes, which is followed by a final decay. There are smaller perturbations in each of the fields, but these are not as well correlated with each other.

The equivalent storm mass and layer masses (Figure 5) have similarities to the volume/area curves of Figure 4, but there are also some rather distinct differences. All three curves plus that for the reflectivity maxima correlate well with each other. There is a marked increase in the first 75 minutes followed by a decay and another peak about 260 minutes, as seen in the volume/area data. There is also a minimum in both the volume and mass data about 135 min, followed by a relatively minor peak about 150 min. A major difference is that the dominant peak in the mass curves is at 75 min not at 260 min as seen in the volume data.

The greatest variability with time is seen in the height plots of Figure 6. Here are plotted heights of the echo top, mass-weighted centroid, maximum reflectivity factor, and the levels of maximum area and mass. The centroid height is the most stable of the curves, having distinct peaks at 60 and 140 minutes, slightly leading the maxima seen in the volume and mass curves of Figures 4 and 5. The heights of the maximum Z and the level of maximum mass are highly correlated, as would be expected since these parameters are dependent.

The loci of the locations of the maximum in reflectivity factor, the echo tops, and the storm centroid (Figure 7) tend to track quite consistently, with the centroid track having the smoothest appearance. The echo top is always located to the south of the centroid track. This suggests that the primary updraft is located on the south side of the storm. The location of the maximum reflectivity factor shows much greater fluctuation and is probably quite unreliable as a storm indicator.

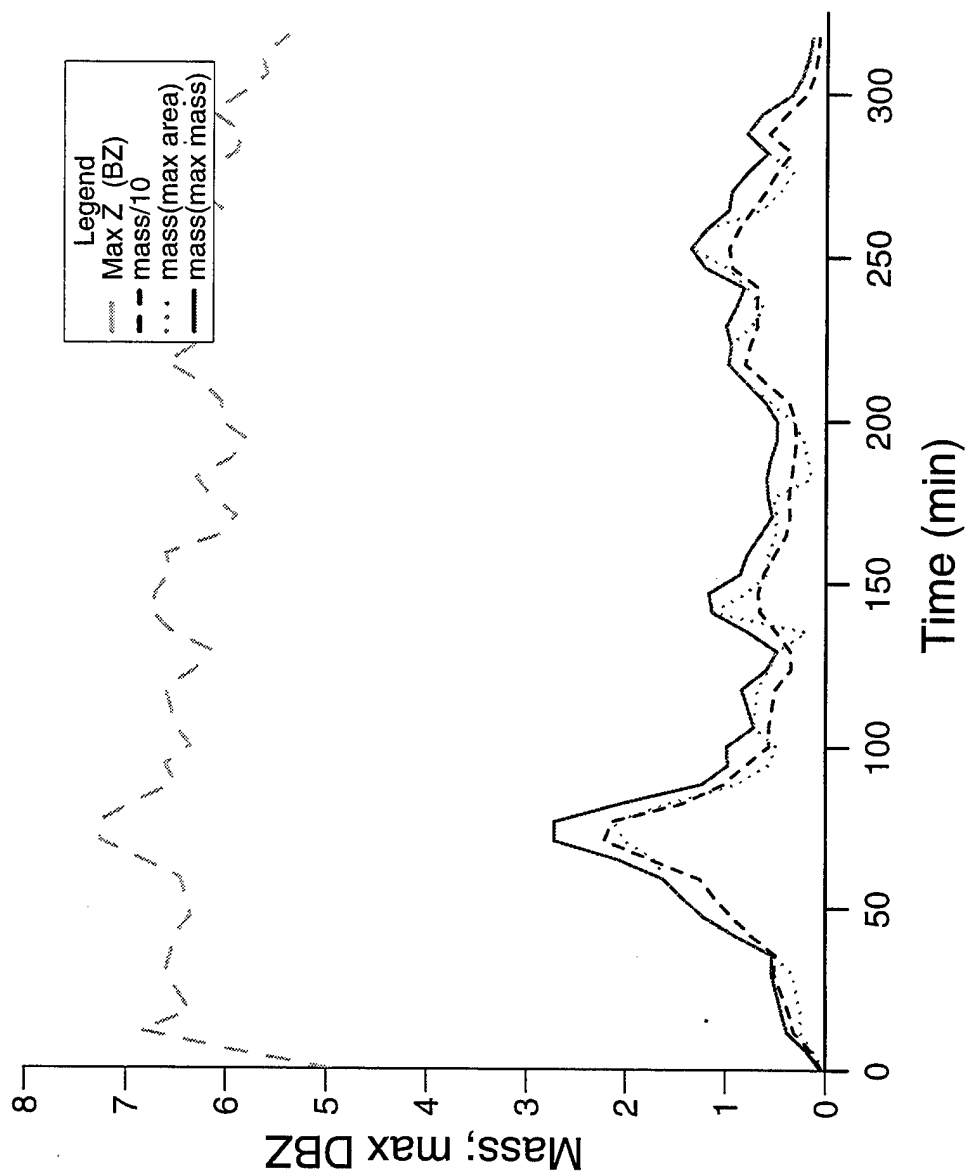


Figure 5. Plot of storm precipitation mass, maximum reflectivity factor, and the masses within the layers where the area and masses are maxima as a function of time. Data are for Dodge City data for May 16-17. Time is as in Figure 3.

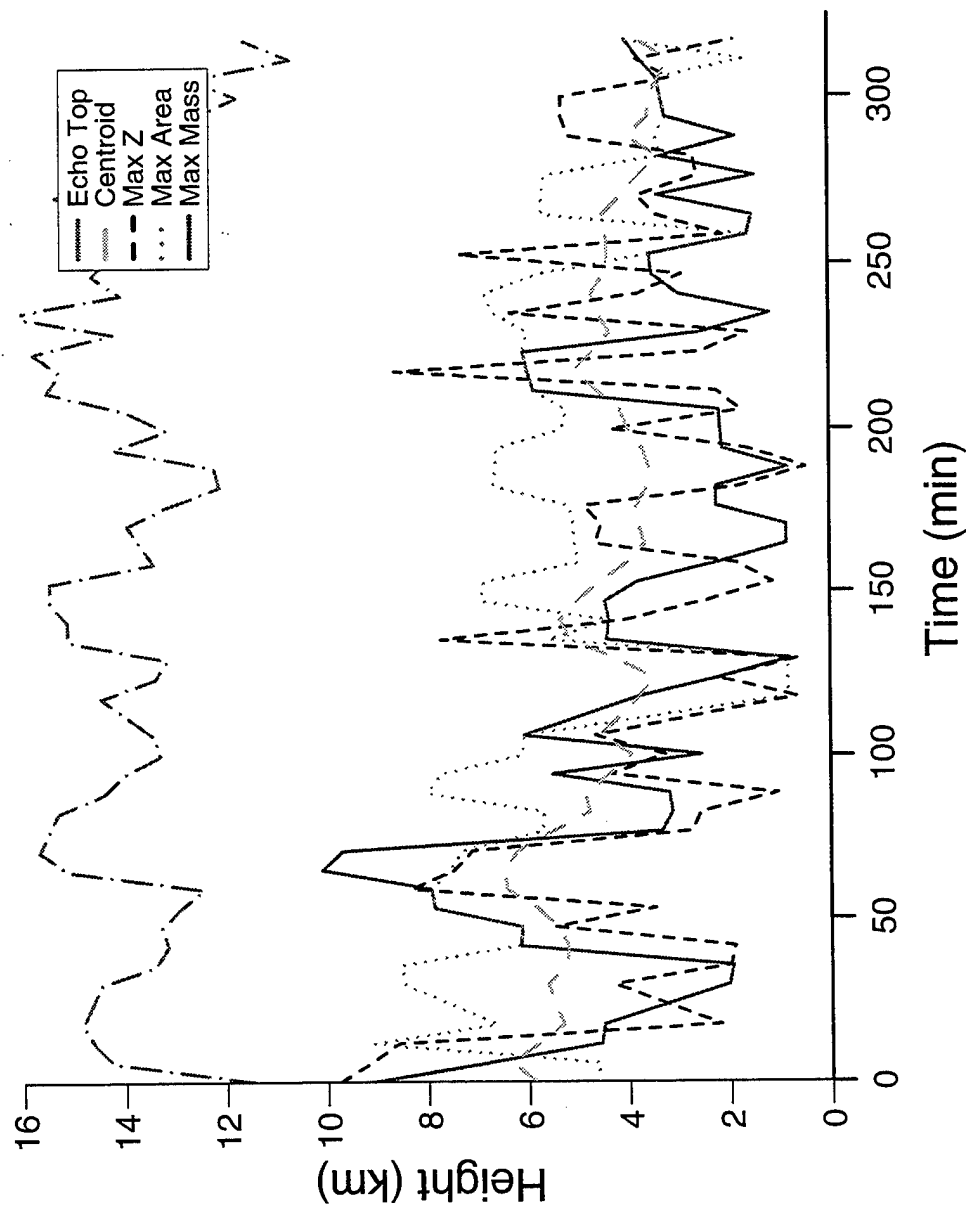


Figure 6. Plots of the heights of the echo top, storm centroid, maximum reflectivity, the layer with the greatest area, and the layer with the greatest mass as a function of time. Data are for Dodge City data for May 16-17. Time is as in Figure 3.

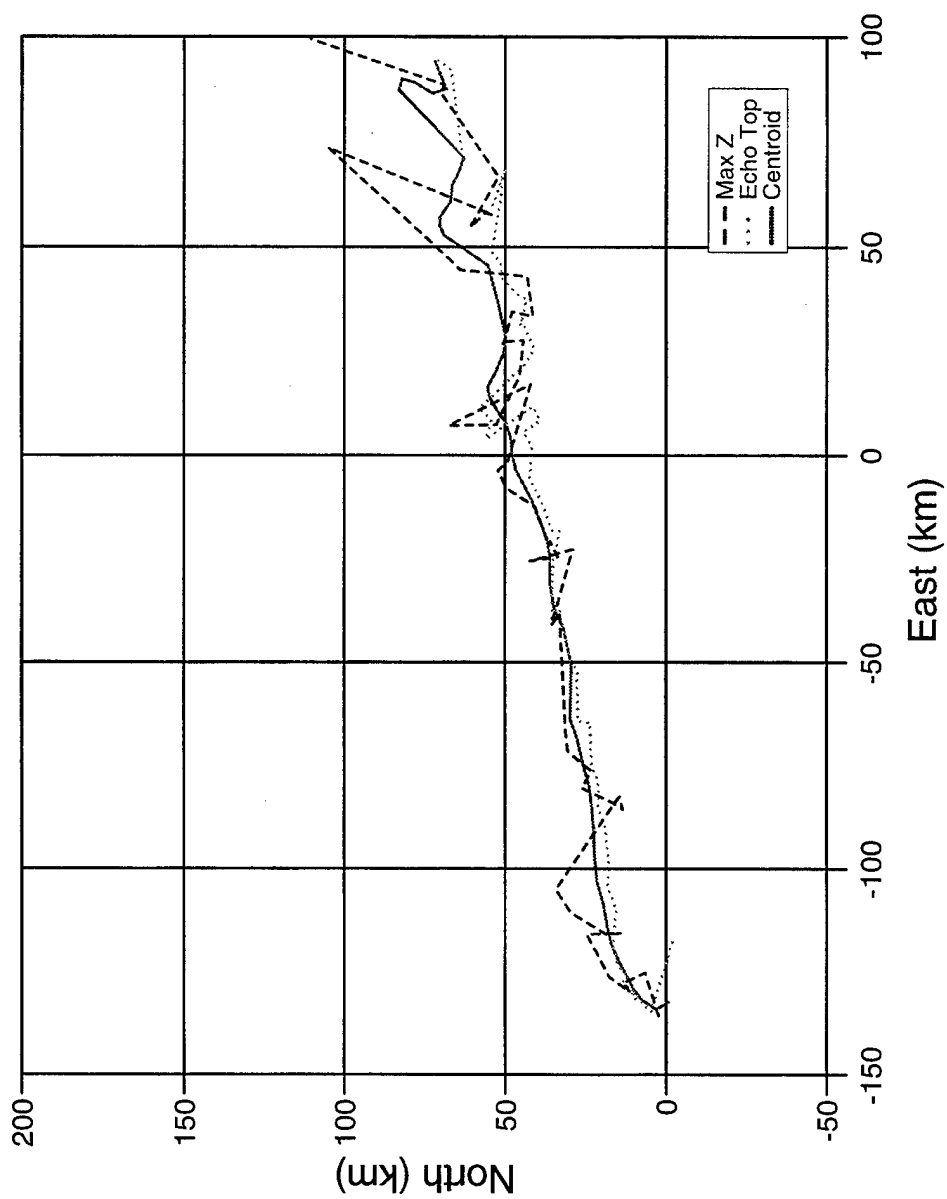


Figure 7. Plots of the locations relative to the radar of the maximum reflectivity factor, echo top, and the sotrm centroid. Data are for Dodge City data for May 16-17.

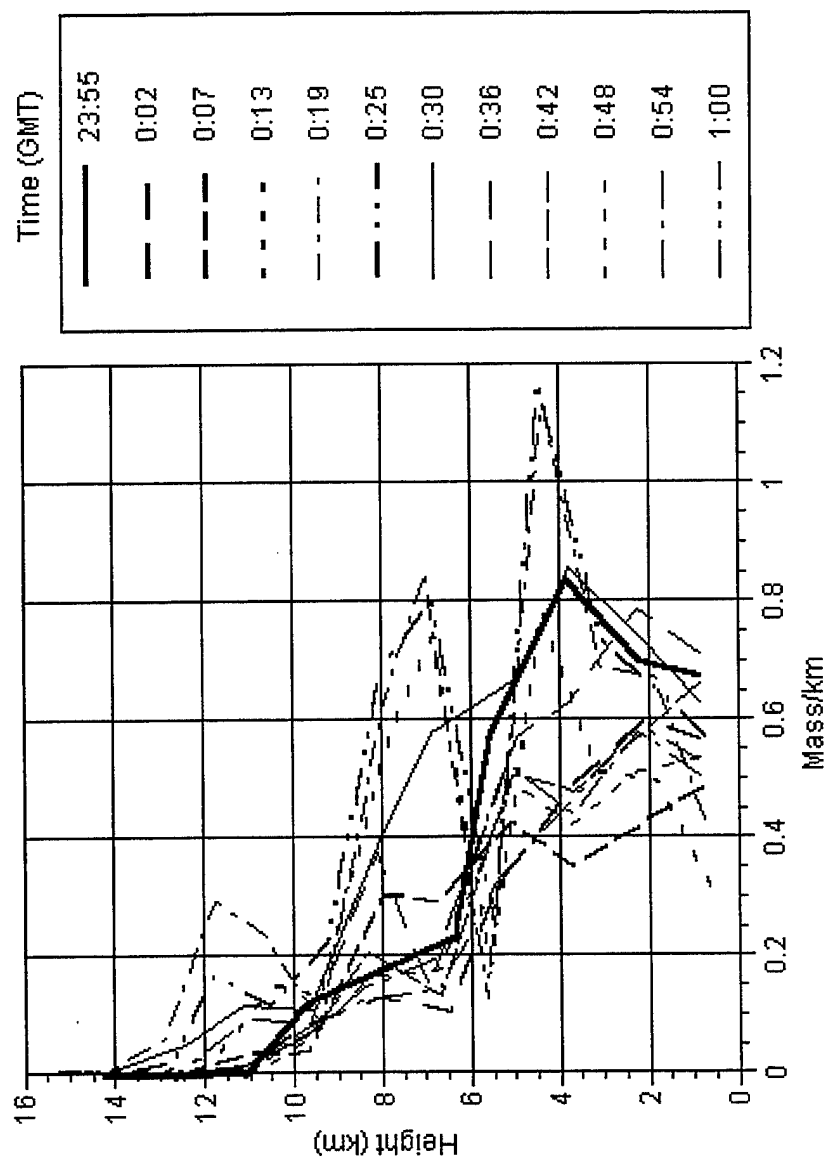


Figure 8. Height profiles of the mass in 1 km layers for a series of radar volumes at times as in the figure legend. Profiles are for Dodge city data for May 16-17, 1995.

Figure 8 contains height profiles of normalized layer mass for a number of volume scans. These profiles correspond to the 118 to 183 min. period of the previous figures, a generally “quiet” period. In these profiles we see the collapse of the water mass aloft to the lower levels and then a decline at all levels. Towards the end of the period, there is the start of a buildup about 8 km height, leading up to the subsequent development seen in the other plots. This type of plot needs to be further explored, especially when assessing lightning potential.

Table 1. Storm Data Relating to Dodge City Storm

Time (UTC)	Relative Time	Hail	Tornado
2306	69	1.00	
2310	73	1.50	
2316 - 2335	79 - 98		F3
2316	79	1.00	
2320	83	4.50	
2323	86	2.75	
2340 - 2345	103 - 108		F0
2350	113		F0
0000	123	1.50	
0009	132	0.88	
0015	138	1.25	
0024	147	1.75	
0026	149	1.00	
0036	159	0.75	
0038	161	1.75	
0045 - 0048	168 - 171		F0
0046	169	1.75	
0049 - 0054	172 - 177		F0
0050	173		F0
0112 - 0124	195 - 207		F0
0139 - 0144	222 - 228		F2
0146 - 0230	229 - 265		F3
0157 - 0205	240 - 248		F0

In Table 1 are the times (in UTC and in the coordinates used in Figures 3 - 7) of the tornadoes and hail occurrences associated with this storm. The numbers in the hail column indicate hail diameter in inches and the scale in the tornado column refers to the Fujita intensity scale for tornadoes. Note that the most significant hail and tornado activity occur in the period from about 75 to 110 minutes. This is the time frame when the volume of the storm was at a relative maximum (Figure 4) and the mass was decreasing (Figure 5). Echo

top was descending as were the heights of the centroid and all mass related parameters (Figure 6). It would appear that the rapid growth in precipitation characteristics may be an indicator of impending severe weather. Once severe weather has been initiated the relationships between subsequent occurrence within that storm and these indicators are much less conclusive.

4.2 May 12, 1995 Goodland, KS

In many respects this storm is quite similar to the Dodge City storm described above. It is a long lived (over 5 hours) eastward moving storm that produces several small tornadoes and a significant amount of hail of diameters greater than 1.75 inches. This storm had a long-lived weak echo region which Smalley *et al* (1996) tracked for over 90 minutes. As seen in Figs 9 and 10, the Goodland storm starts slowly and then gradually increases both in mass and volume, with the greatest values at the end of the observing period. In both of these plots there appear to be pulsations in intensity as was seen in the Dodge City case.

Figure 11, the plot of area and mass versus height and time is also quite similar to Figure 3, that for the Dodge City case. The largest area at any time tends to be elevated, with the height increasing markedly after 240 minutes. Precipitation mass tends to be concentrated more in the lower levels of the storm but with the height increasing after 240 minutes. The height rises during the last approximately third of the time period are artifacts of the distance of the storm from the radar. At long ranges, the radar no longer sees the lower portions of the storm.

Figure 12 shows the volume and layer area statistics as in Figure 4. For the first 200 minutes, there is excellent correlation between the curves. Beyond that range, the area of the maximum mass layer tends to fluctuate much more than the volume and the area of the maximum area layer. This again is probably an artifact due to the distance of the storm from the radar. During the earlier time period, there are fluctuations in these curves at 30 minute intervals, again similar to the Dodge City case.

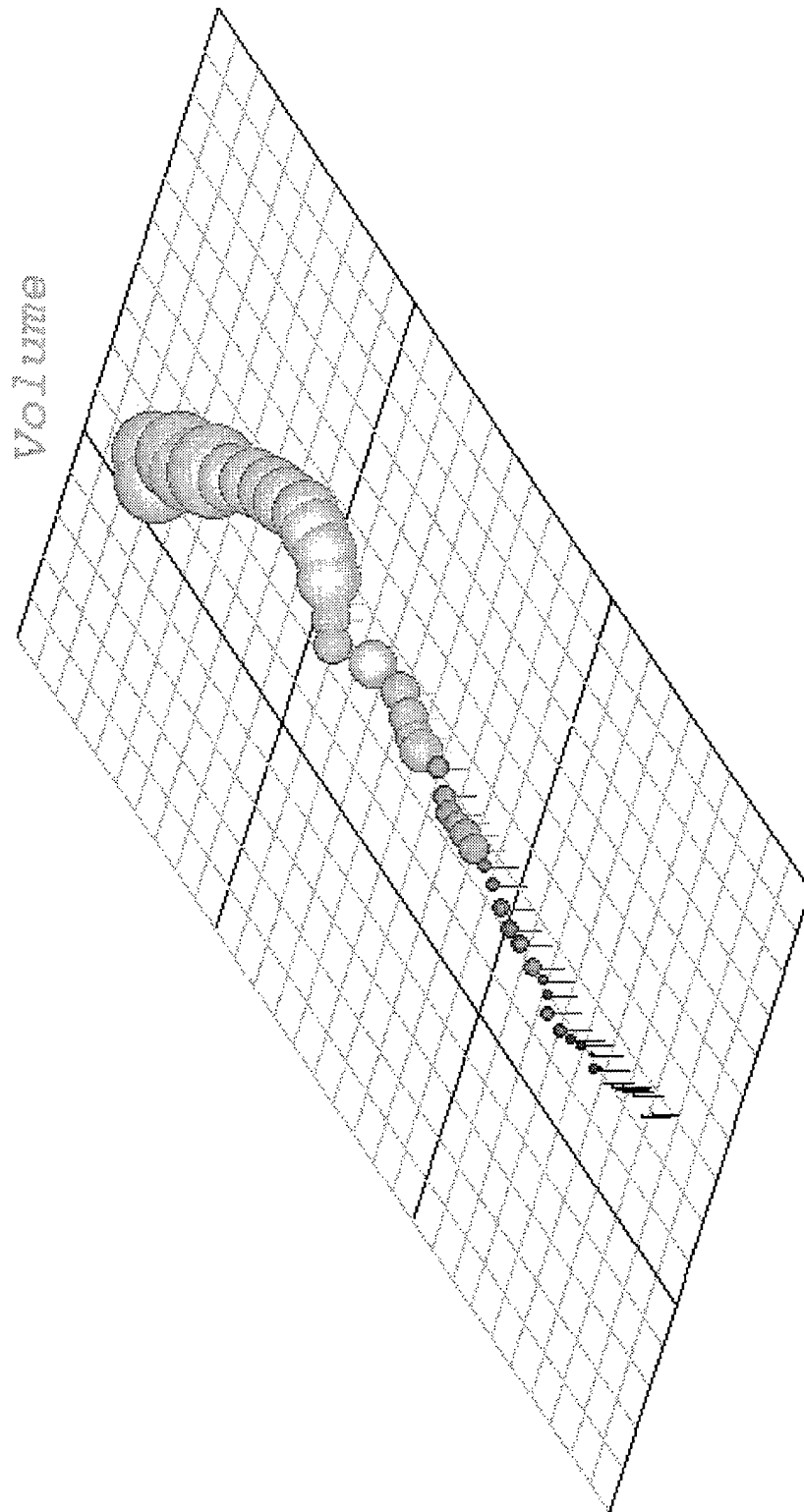


Figure 9. As in Figure 1 but for data collected by Goodland, Ks WSR-88D radar on May 12, 1995.

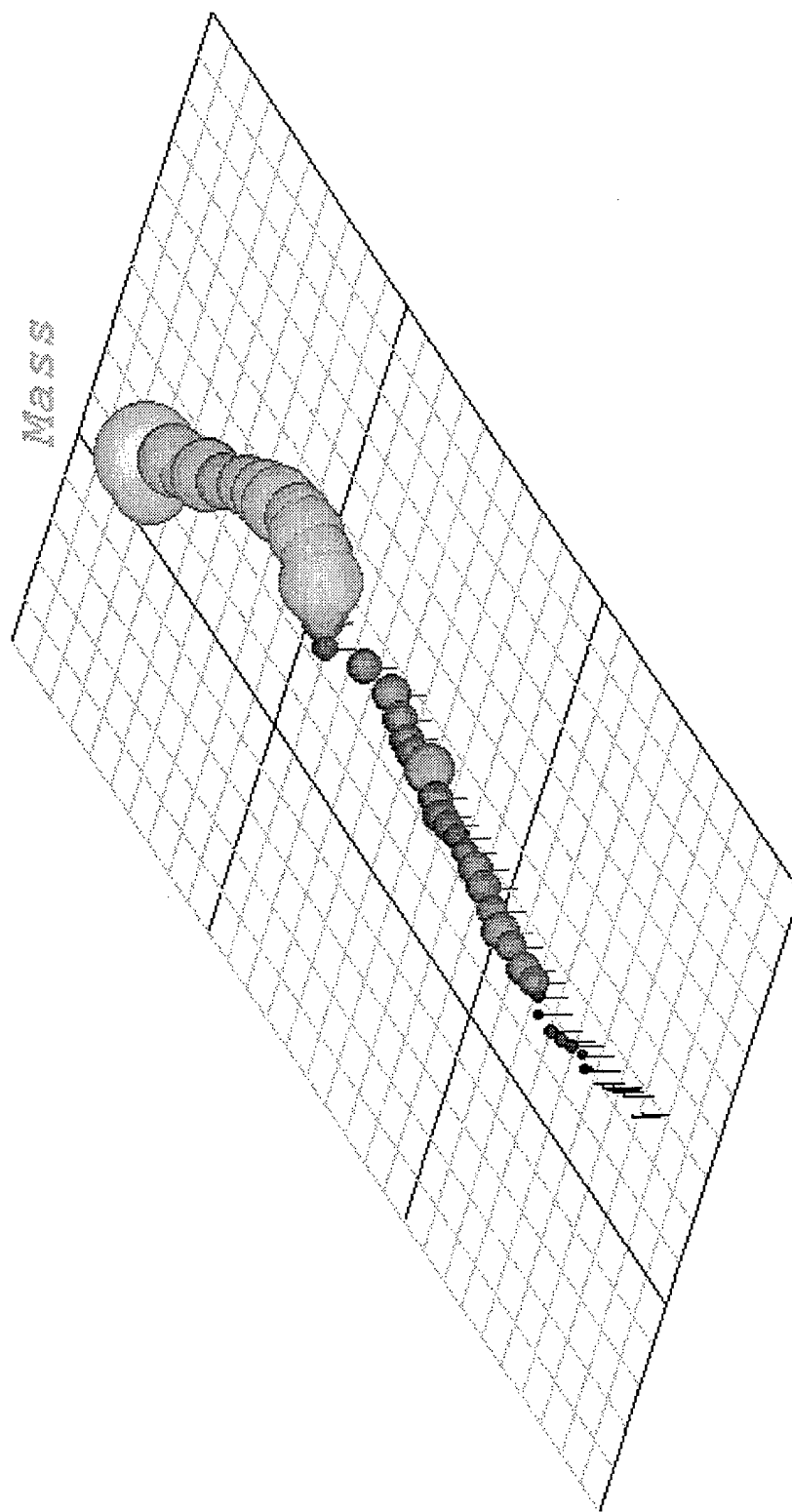


Figure 10. As in Figure 2 but for data collected by Goodland, KS WSR-88D radar on May 12, 1995.

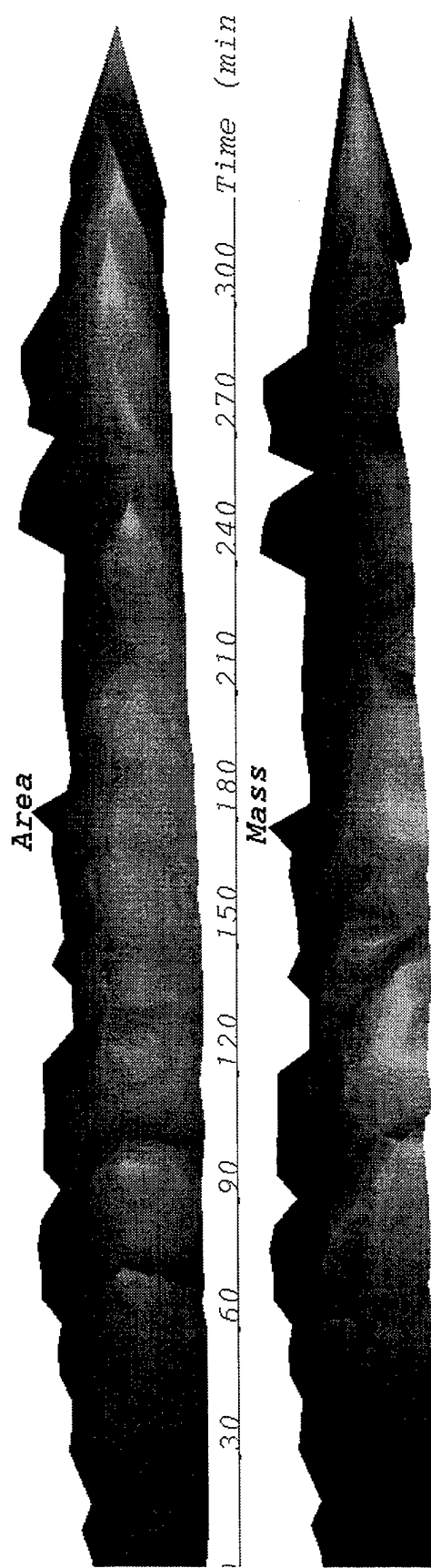


Figure 11. As in Figure 3 but for data collected by Goodland, KS WSR-88D radar on May 12, 1995.

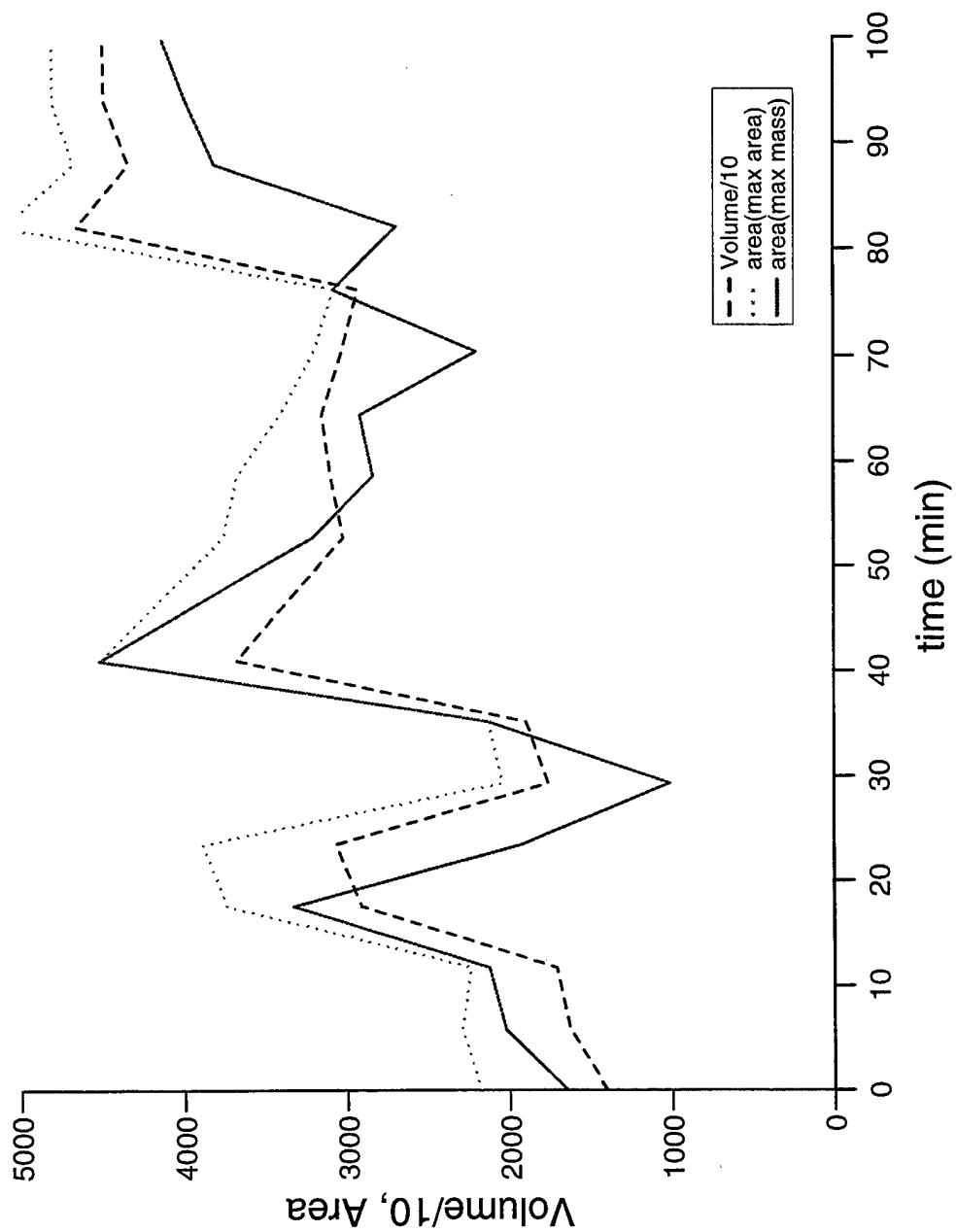


Figure 12. As in Figure 4 but for data collected by Goodland, KS WSR-88D radar on May 12, 1995.

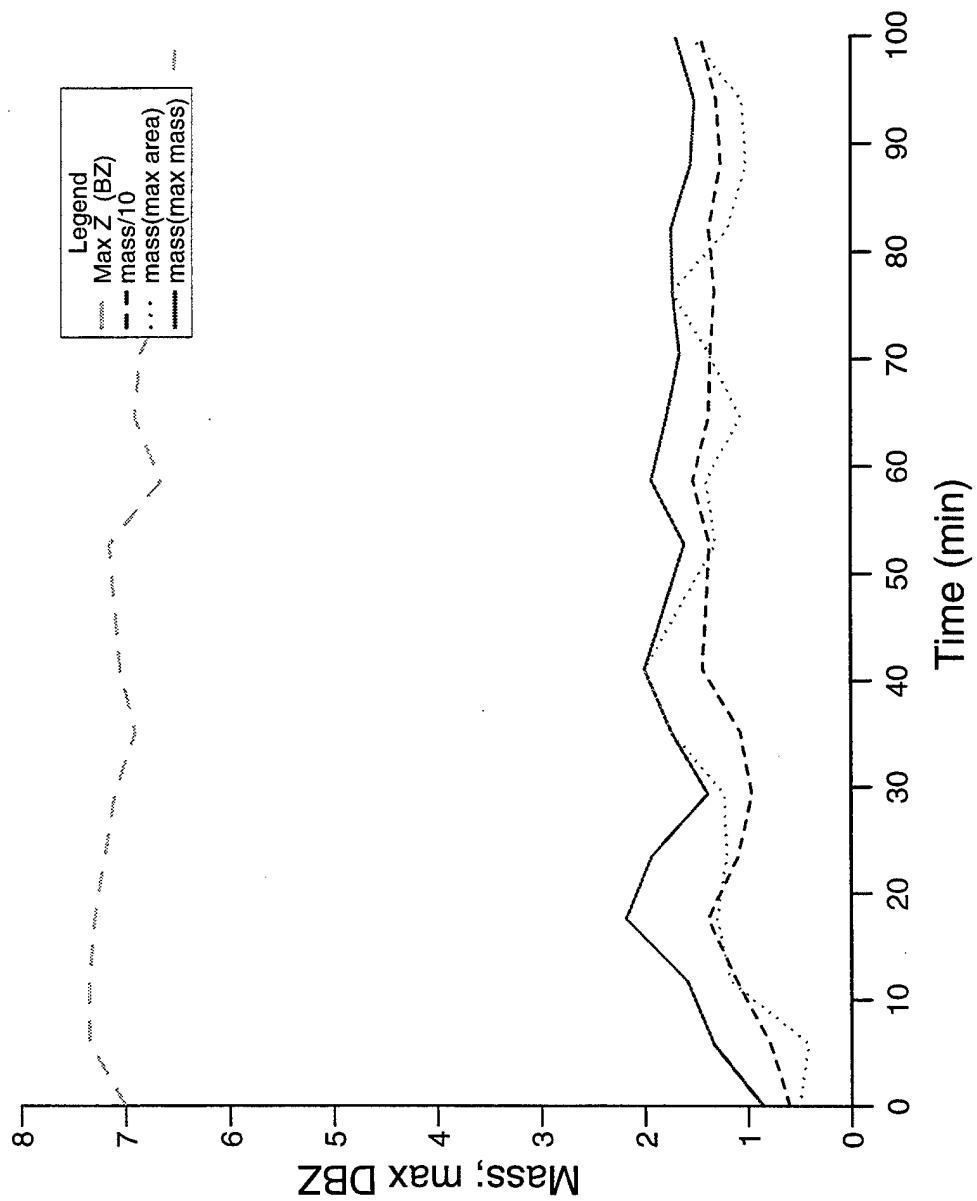


Figure 13. As in Figure 5 but for data collected by Goodland, KS WSR-88D radar on May 12, 1995.

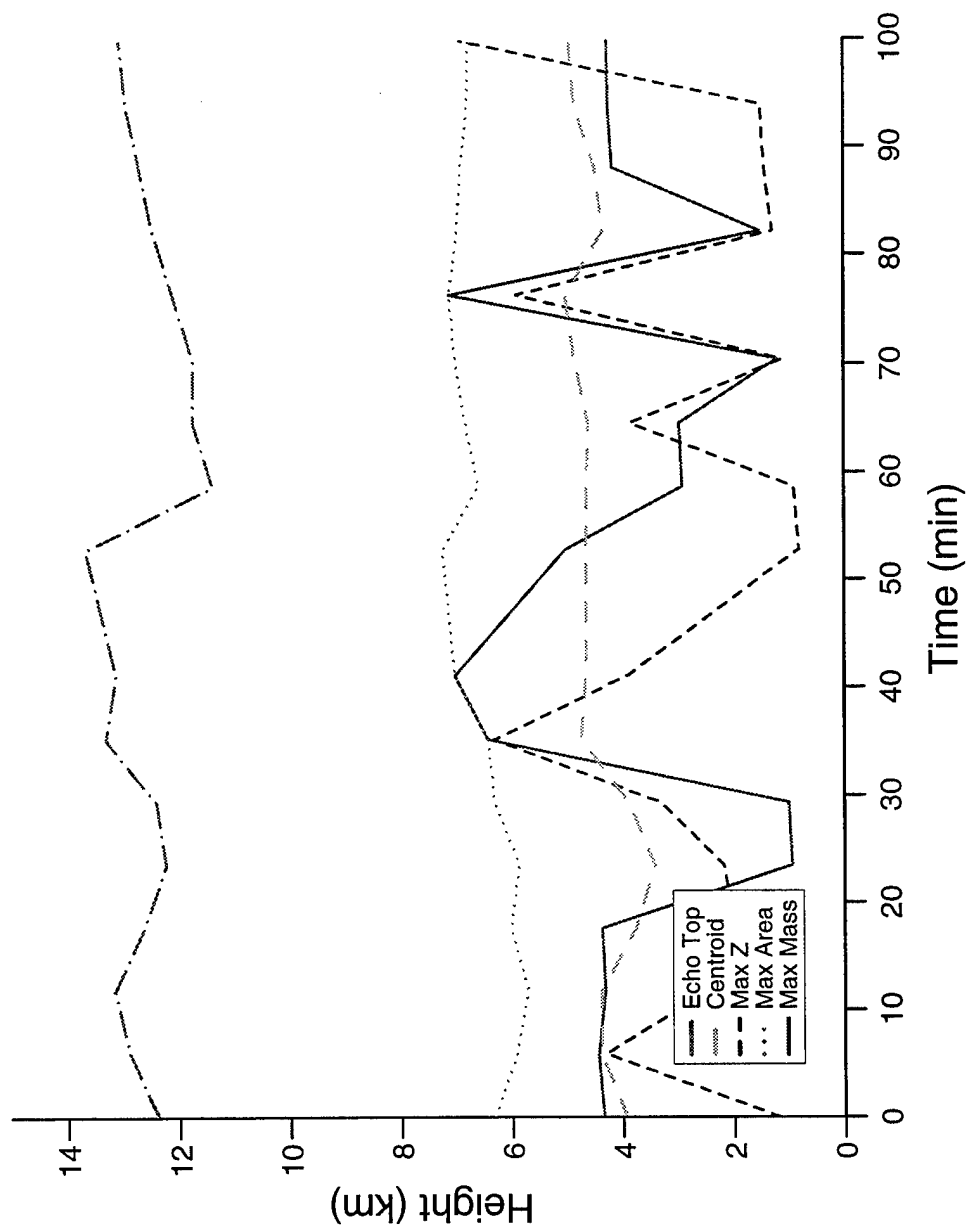


Figure 14. As in Figure 6 but for data collected by Goodland, KS WSR-88D radar on May 12, 1995.

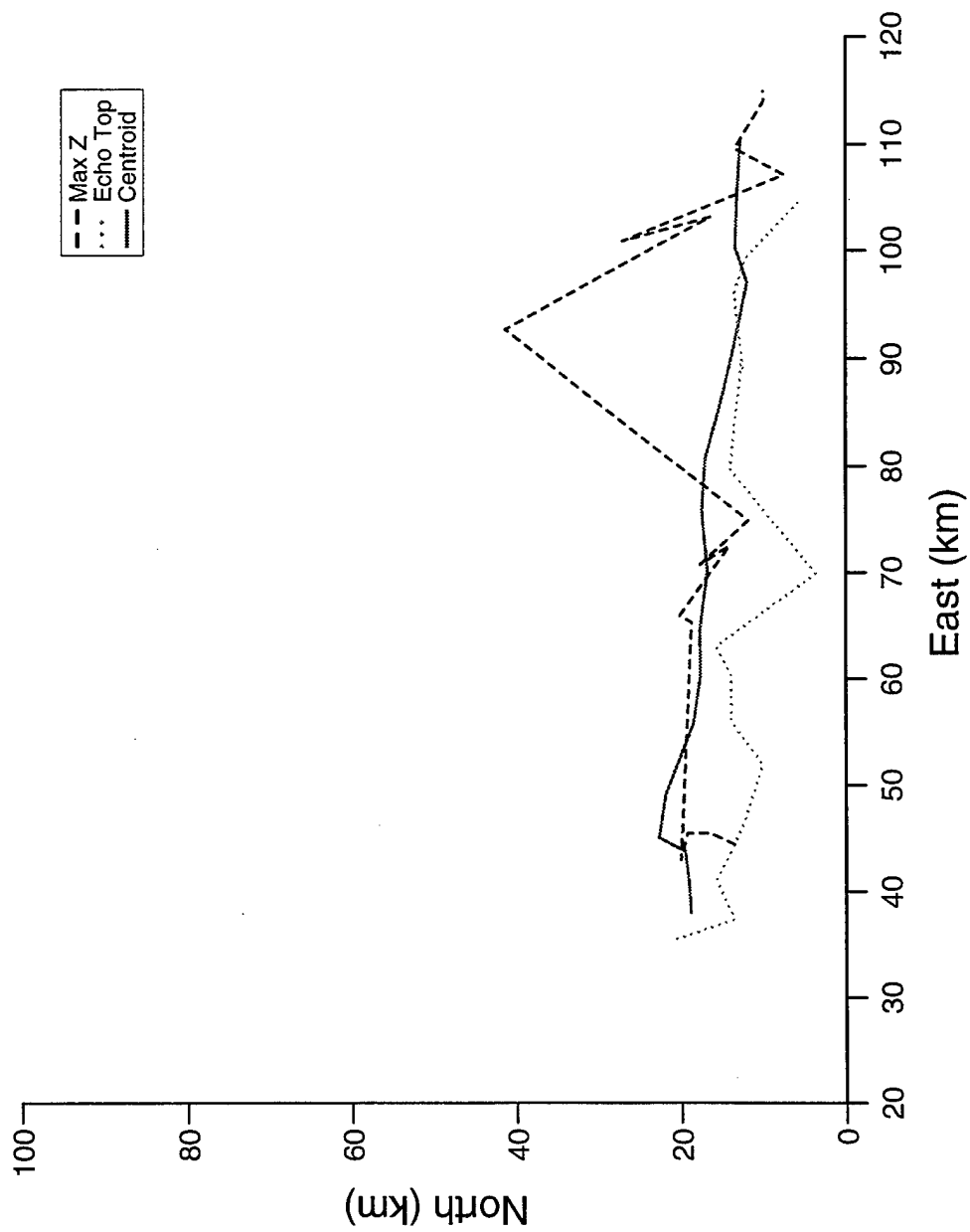


Figure 15. As in Figure 7 but for data collected by Goodland, KS WSR-88D radar on May 12, 1995.

The mass and maximum reflectivity factor curves (Fig 13) show a similar trend to the area curves but appear to be slightly better behaved. The periodicity in these curves is closer to 15 minutes, about one-half that for the area data.

The height curves in Figure 14 (similar to those in Figure 6) have marked fluctuations in each, but there is little correlation amongst the curves. They all, however, show a marked upward tendency with time after 150 minutes. This is again a function of the storm position with respect to the radar.

Table 2. Storm Data Relating to Goodland, KS Storm.

Time (UTC)	Relative Time (min)	Hail	Tornado
1940	60	2.5	
1955	75	1.75	
2000	80	0.75	
2000	80	1.75	
2010	90	1.50	
2012	92		F0
2015 - 2100	95 - 140		F2
2030	110	1.75	
2050	130	1.75	
2055	135	2.50	
2100 - 2135	140 - 175		F2
2112	152	1.75	
2130	170	1.00	
2145 - 2147	185 - 187		F2
2150 - 2151	190 - 191		F1
2150	190	1.00	
2158	198	1.75	
2200	200	2.75	
2204	204	1.00	
2218	218	1.75	
2235	235	1.00	
2241	241	2.00	

The positions plotted in Figure 15 are similar to those in Figure 7. The most stable track is that for the storm centroid while that for the maximum reflectivity factor is the most erratic. The echo top is also always located south of the centroid.

Table 2 contains the hail and tornado information that is available for this storm. The first (and largest) hail occurs 60 minutes after the start of observations, the time of the first peak in the volume data (Figure 12) and the mass data (Figure 13). Storm top and centroid (Figure 14) are continuing to rise while the other height parameters show no clear pattern. The next hail occurrence is near the time of the second peak in each of the mass and volume plots. The tornadoes that are initiated at 92 and 95 minutes appear to occur when there has been a sharp decrease in both the mass and volume sets of plots. However, the rest of the tornado activity does not appear to bear any correlation with the reflectivity structure assessment as presented in Figures 9 to 14. There does appear to be a loose correlation between the occurrence of large hail and peaks in the mass curves. This relationship deserves closer attention in the future.

5 SUMMARY

An analysis scheme has been developed that will provide assessments of the precipitation structure within storms. This algorithm will serve as the basis for a lightning precursor algorithm. For this report, this algorithm has been applied to two storms that produced severe weather in the form of large hail and several weak to moderate tornadoes. Results appear to be promising in terms of giving indications of the occurrence of large hail and of the occurrence of the first tornado. It should also be noted that Smalley *et al*, 1996 have also used this algorithm to evaluate the structure of weak echo regions. During the last year of this contract, this algorithm will be applied to data for which there are lightning data and an evaluation of the various output parameters that are available from this package will be assessed as lightning precursors. It should be noted that, in this presentation, not all available output parameters have been presented since the relevance of those that have been omitted to a more general severe storm analysis has yet to be determined.

6 REFERENCES

- Beuchler, D.E., and S.J. Goodman, 1991: Radar characteristics of cloud-to-ground lightning producing storms in Florida. Preprints, 25th Conf. on Radar Meteorol., Amer. Meteorol. Soc., 897 - 900.
- Harris-Hobbes, R., M. Bellmore, A. Lunsford, and K.L. Giori, 1992: Radar determined stand-off distances for use in the launch commit criteria - final report. NASA contract Rpt., Contract No. NAS10-11853, Aeromet, Inc., 51p.
- Holle, R.L., A.I. Watson, R.E. Lopez, K.W. Howard, R. Ortiz, and L.Li, 1992: Meteorological studies to improve short-range forecasting of lightning/thunderstorms within the Kennedy Space Center area. NSSL Final Report for Mem. of Agreement between the Office of Space Flight, NASA and the National Severe Storms Laboratory, 91p.
- Krehbiel, P., 1986: An animated comparison of the lightning charge transfer and radar reflectivity in a Florida thunderstorm. Preprints, 23rd Conf. on Radar Meteorol., Amer. Meteor. Soc., J294 - J295.
- Lhermitte, R., and P. Krehbiel, 1979: Doppler radar and radio observations of thunderstorms. IEEE, vol. GE-17, pp 162-171.
- Marshall, T.C., and Radhakant, 1978: Radar precipitation maps as lightning indicators. J. Appl. Meteorol., 17, 206-212.
- Smalley, D.J., F.I. Harris, S-L. Tung, and A.R. Bohne, 1996: Radar Studies of Aviation Hazards: Part 1. Storm Structure Algorithm, PL-TR-96-2178(I).
- Williams, E.R., 1991: The structure of tropical convection and its contribution to the global electrical circuit. Preprints, 25th Conf. on Radar Meteorol., Amer. Meteorol. Soc., 893 - 896.